RSC Advances

ROYAL SOCIETY OF CHEMISTRY

www.rsc.org/advances

RSC Advances

COMMUNICATION

Hydrothermal generation of compressed hydrogen gas by iron powders

Received 00th January 20xx,
Accepted 00th January 20xx

DOI: 10.1039/x0xx00000x

www.rsc.org/

Yu-Ching Tsai, Liang-Hsing Liu and Dong-Hwang Chen*

Compressed hydrogen gas has been generated from water and iron powders via hydrothermal method. As compared to the conventional steam-iron process, this process has the advantages of low temperature, simplicity, and high purity. Also, the direct generation of compressed hydrogen gas was favorable for its storage and utilization.

Because the energy shortage and the greenhouse effect are getting more serious, the development of alternative energy resources such as biofuel, solar energy, hydroelectric power, wind electric power, geothermal electric power, and hydrogen energy has become an important issue nowadays.[1–5] Hydrogen gas is an environment friendly fuel because its reaction product with air is water only. Also, it has wide and abundant sources, including water, fossil fuel, biomass, and hydride. Therefore, hydrogen energy has become one of the most potential alternative energies in the last decade.[5–8] Hydrogen gas can be produced by many different methods such as light/dark fermentation, fossil fuel reforming, hydride decomposition, and water splitting.[7–14] Because water is the most abundant source of hydrogen on the earth and could be regenerated easily, water splitting is particularly attractive. The methods for generating hydrogen gas by water splitting include electrolysis,[15] thermal decomposition,[16] thermochemical cycles,[17,18] solar water splitting,[4,7,19] and the oxidation-reduction of metals and water.[20–30] The method based on the oxidation-reduction of metals and water has received considerable attention because the other methods usually have the disadvantages of high cost, high energy consumption, poor efficiency, or harmful byproducts. The metals used commonly included aluminum, iron, zinc, nickel, etc.[20–30] Steam-iron process is a conventional technique for the generation of hydrogen gas by using the reaction of iron powder and water vapor. The corresponding reaction equation is as follows:[27–30]

$$3Fe + 4H_2O \rightarrow Fe_3O_4 + 4H_2 \quad (1)$$

From this process, pure hydrogen gas can be obtained without other pollutant byproducts. However, this process needs water vapor and has to be performed at a high temperature (> 600 K), leading to the higher energy consumption and process complexity.[27–30]

In this study, we developed a facile hydrothermal process for the generation of compressed hydrogen gas via the reaction of water and iron powders. As compared to the conventional steam-iron process, the process developed in this work has the advantages of simplicity, lower temperature, and high purity. Also, the generation of compressed hydrogen gas was favorable for its storage and utilization. It is expected to be useful for the developments of hydrogen gas generation techniques and the hydrogen energy-related devices (such as fuel cells) or chemical processes.

The hydrothermal generation of hydrogen gas was conducted in a Teflon-lined stainless steel autoclave connected with a hydrogen gas collection bottle. In general, an appropriate amount of iron powders and 40 mL of pure water were put into the cylinder reactor of 100 mL. By heating the reactor, hydrogen gas was generated. The temperature and pressure of reaction were measured by a thermocouple and a pressure detector system, respectively. To establish the appropriate operation condition, the effects of reaction temperature, iron powder amount, and the size and morphology of iron powders were examined. Spherical iron powders of 100 nm were purchased from US Research Nanomaterials, Inc. Spherical iron powers of 3 μm were provided by Chung-Shan Institute of Science & Technology, Republic of China. Flat iron powers of 45 μm and 60 mesh were the products of J. T. Baker and Wogonin Wako Pure Chemical Industries, Ltd., respectively. After reaction, the switch between the autoclave and the hydrogen gas collection bottle was opened and the hydrogen gas generated was discharged to the collection bottle for characterization by gas chromatography (Shimadzu GC-2014). The solid powders were washed with deionized water several times and then dried in a vacuum oven. Their change in the crystalline structures before and after reaction was characterized by X-ray diffraction (XRD;

Department of Chemical Engineering, National Cheng Kung University, Tainan, Taiwan, Republic of China. E-mail: chendh@mail.ncku.edu.tw

Shimadzu model RX-III) using Cu Kα radiation at an acceleration voltage of 40 kV and a current of 40 mA. The changes in morphology and size were characterized by a high resolution field emission scanning electron microscope (HR-FESEM, JSM-6700F).

To demonstrate the feasibility of hydrothermal generation of hydrogen gas by iron powders and water, water and different amounts of 3 μm iron powders (0, 10, 20, and 30 wt%) were reacted at 120°C. As shown in Fig. 1, the vapor pressure of pure water remained at only about 1.5 bar. However, in the presence of iron powders, the pressure increased steadily with time and the pressure increase became more obvious with increasing the amount of iron powders, implying hydrogen gas has been generated. By analyzing the composition of collected gas after reaction using gas chromatography, it was found that the water content was only about 0.525%. This revealed that the generated gas was the high purity of hydrogen gas and demonstrated that the hydrothermal process developed in this work was indeed effective in the generation of compressed hydrogen gas with high purity. In addition, Fig. 2 shows the XRD patterns of 3 μm iron powders before and after reaction at 120°C for 9 h. Before reaction, only the characteristic peaks of Fe related to (100) and (200) planes were observed at 2θ=44.7 and 65.1°, respectively. After reaction, the characteristic peaks of Fe_3O_4 corresponding to (220), (311), (222), (400), (422), (511), (440) and (533) planes appeared at 2θ=30.4, 35.7, 37.4, 43.4, 53.8, 57.2, and 74.3°, respectively. It was obvious that Fe has been partially converted into Fe_3O_4 after reaction, providing an evidence for the reaction (1).

To study the effect of temperature on the water vapor and hydrogen gas generation, the variations of pressure with time in the presence and absence of 3 μm iron powders (20 wt%) at different temperatures were measured. As shown in Fig. 3, in the presence of iron powders, the pressure increased steadily with time and the increase was enhanced by increasing the temperature. When the temperature was raised to 150°C, the pressure was over 80 bar after about 7 h. In the absence of iron powders, the vapor pressure of water reached a constant after about 1 h and increased with increasing the reaction temperature as shown in Fig. 3. However, they all were much lower than those in the presence of iron powders. This revealed that the generation of hydrogen gas could be enhanced by increasing the temperature. Furthermore, it was mentionable that the unreacted water vapor could be cooled down and converted back to liquid water after reaction. Thus, even more water vapor was formed at a higher temperature, the generated hydrogen gas could be separated easily from the unreacted mixture and discharged to the collection bottle after reaction.

To investigate the effects of size and morphology of iron powders on the generation of hydrogen gas, four kinds of iron powders were used. As shown in Fig. 4, it was obvious that 100 nm iron powders exhibited significantly faster generation rate than micro-sized iron powders. This could be attributed to the larger specific surface area of nano-sized iron powders which favored the reaction with water. However, it was noted that the flat iron powders of 45 μm had a faster initial hydrogen generation rate than the spherical iron powders of 3 μm. This

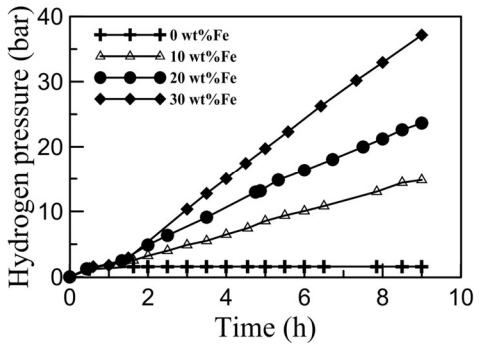

Fig. 1 Variation of pressure with time during the hydrothermal generation of hydrogen gas at 120°C and different amounts of 3 μm iron powder.

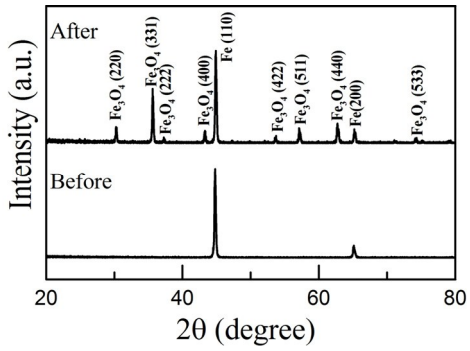

Fig. 2 XRD patterns of 3 μm iron powders before and after reaction at 120°C for 9 h.

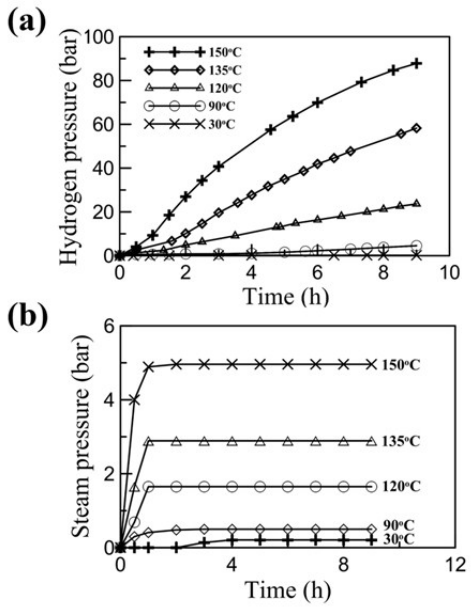

Fig. 3 Variations of pressure with time during the hydrothermal generation of hydrogen gas by 3 μm iron powders (20 wt%) at different temperatures (a) and the corresponding pressure variations with time for water (b).

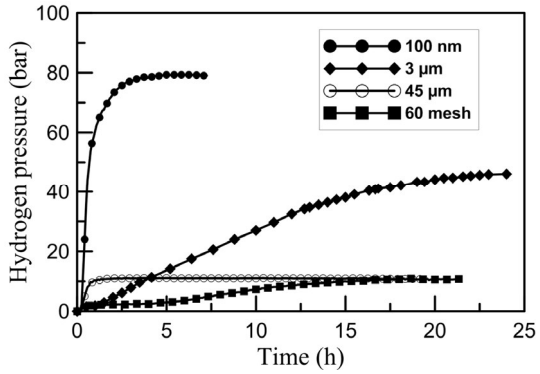

Fig. 4 Variations of pressure with time during the hydrothermal generation of hydrogen gas in the presence of different iron powders (20 wt%) at 120°C.

might be due to the fact that flat powders had a larger surface area than spherical powders.

In addition, it was mentionable that the oxidation of iron powders occurs from the surface to the inner part. The resulting Fe_3O_4 shells might hinder the further oxidation of inner part. So, the conversion might be affected by the reaction temperature, reaction time, and the size and morphology of iron powders. Figure 5 shows the corresponding XRD patterns of different iron powders after reaction. As compared to those before reaction, the conversions of 3 μm, 45 μm, and 60 mesh iron powders after reaction for 24 h were estimated to be 45.1, 12.6, and 12.2%, respectively, according to the decrease in the intensity of Fe(110) peak after reaction. By dissolving 0.1 g of reaction mixture in 20 mL HCl solution and analyzing the iron content using atomic absorption spectrophotometry (GBC SensAA), the conversions of 3 μm, 45 μm, and 60 mesh iron powders after reaction for 24 h also could be estimated to be 42.8, 13.3, and 13.0%, respectively. They were in agreement with the above XRD analysis. Moreover, according to the decrease in the intensity of Fe(110) peak after reaction, the conversion of 100 nm iron powders after reaction for 9 h could be estimated as 73.3%. However, it was noted that the pressure almost remained unchanged when the reaction time was above about 5 h. This might be due to the fact that the surface oxidation of iron powders might hinder the further reaction of water and inner iron, leading to the incomplete conversion. This also could account for the fact that the flat iron powders of 45 μm showed a fast initial hydrogen generation rate but the conversion almost remained at a low level after 1 h.

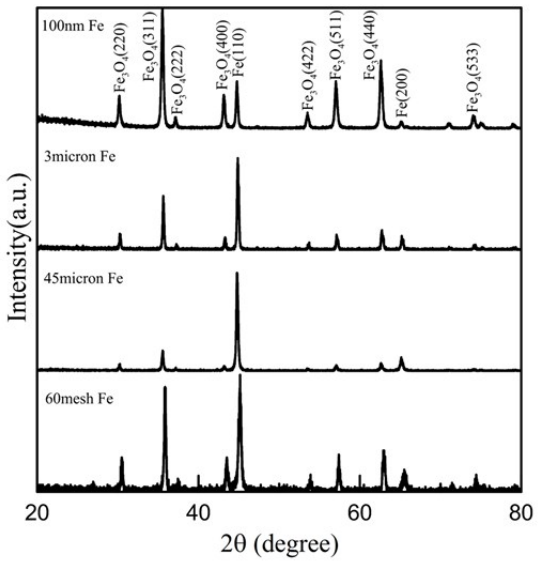

Fig. 5 XRD patterns of iron powders (20 wt%) after reaction at 120°C for 9 (100 nm) or 24 h (3μm, 45μm, and 60 mesh).

Because 100 nm iron powders exhibited the fastest generation rate of hydrogen gas, the corresponding temperature effect was further examined. As shown in Fig. 6, the generation of hydrogen gas was still quite significant even the temperature was lowered to 90°C. When the reaction temperature was raised to 150°C, the generation rate could be further enhanced but the enhancement was not tremendous. Moreover, the reaction was completed after only about 3 h for the case at 150°C but the time required to complete the reaction for the case at 120°C was over 6 h. In addition, Fig. 7 shows the XRD patterns of 100 nm iron powders before and after reaction at 90, 120 and 150°C. It was obvious that Fe was converted into Fe_3O_4 after reaction, and the conversion increased with increasing the temperature. According to the decrease in the intensity of Fe(110) peak after reaction, the conversions for the reaction at 90 and 150°C also could be estimated as 60.7 and 75.2%, respectively. This was consistent with the above hydrogen generation phenomenon as observed in Fig. 6.

Fig. 8 shows the SEM images of different iron powders before and after reaction. It was found that a lot of smaller fragments were formed for 3 μm, 45 μm and 60 mesh iron powders. This might be due to the oxidation of iron powders. However, for 100 nm iron powders, particle aggregation occurred after reaction. This could be attributed to the nature of nanoparticles easy to aggregate owing to their large specific surface energy.

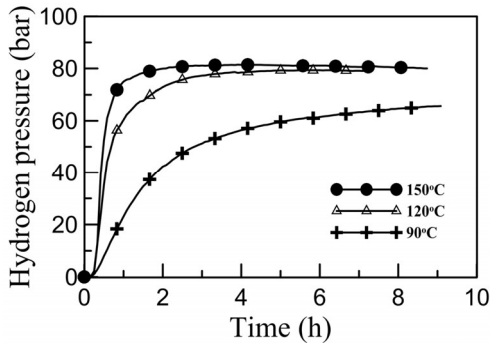

Fig. 6 Variations of pressure with time during the hydrothermal generation of hydrogen gas in the presence of 100 nm iron powders (20 wt%) at different temperatures.

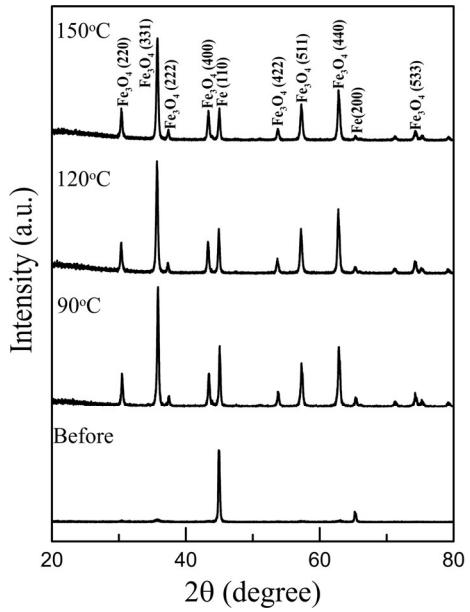

Fig. 7 XRD patterns of 100 nm iron powders before and after reaction at different temperatures.

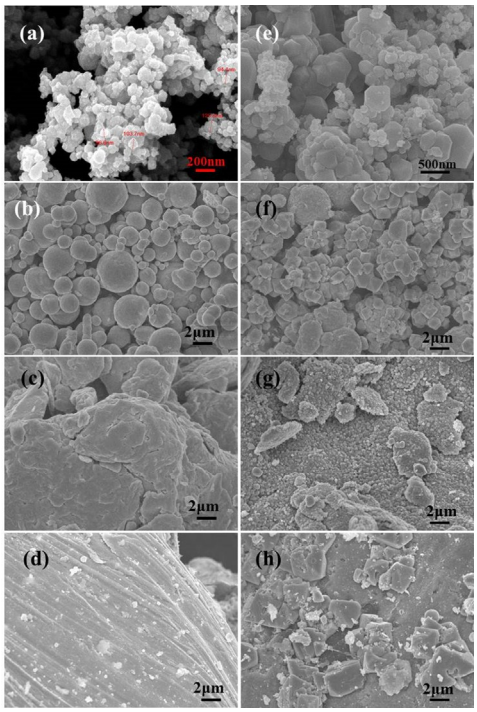

Fig. 8 SEM images of different iron powders before (a–d) and after (e–h) reaction. (a,e) 100 nm, (b,f) 3μm, (c,g) 45μm, (d,h) 60 mesh.

According to the above, the hydrothermal generation process of compressed hydrogen gas by iron powders developed in this work has been demonstrated to be successful. As compared to the conventional steam-iron process, this novel process has the advantages of low temperature (energy saving), simplicity, high efficiency, high purity, and high pressure. In addition, it was mentionable that Wang et al. reported the generation of hydrogen gas by the reaction of water and 200 mesh iron powders in an autoclave recently.[31] However, the reaction temperature was still up to 573 K and HS^- was present as the catalyst. Chen et al. also studied the generation of hydrogen gas by the reaction of 60 nm iron nanoparticles and water at room temperature.[32] However, the generation rate of hydrogen gas was quite slow. Although using the bimetallic nanoparticles of iron and metal catalysts such as Pd, Ni, Cu and Ag could enhance the generation rate, the high cost and poor stability of iron or its bimetallic nanoparticles still limited their practical application.[32] Thus, the hydrothermal generation process of compressed hydrogen gas developed in this work should be more efficient and practicable than the conventional steam-iron process and other iron-based similar processes.

Conclusions

In conclusion, we have successfully developed a novel and facile hydrothermal process for the generation of hydrogen gas by the reaction of iron powders and water. Four iron powders with different sizes and morphology were used. It was observed that the iron powders with smaller size or a flat morphology exhibited faster hydrogen generation rate and higher conversion. Also, the generation rate of hydrogen gas could be raised by increasing the iron powder amount and reaction temperature. After reaction, it was demonstrated that iron powders were oxidized from Fe to Fe_3O_4 and the gas collected was the high purity hydrogen gas. Because of the advantages of low temperature, simplicity, high efficiency, high purity, and high pressure, such a novel and facile hydrogen gas generation technique might find potential applications in hydrogen energy-related devices and hydrogen gas-related chemical processes.

Acknowledgements

This work was supported by the National Science Council of the Republic of China (grant number NSC 103-ET-E-006-004-ET), and the helpful suggestion from Dr. Jan Rogut was deeply appreciated.

References

1 Y. Zhou, M. Hejazi, S. Smith, J. Edmonds, H. Li, L. Clarke, K. Calvin and A. Thomson, *Energy Environ. Sci.,* 2015, **8**, 2622–2633.
2 M. ShervinZakeri and M. M. Taghizadeh, *Tech. J. Engin. App. Sci.*, 2014, **4**, 120–123.
3 J. Lü, C. Sheahan and P. Fu, *Energy Environ. Sci.,* 2011, **4**, 2451–2466.
4 P. D. Tran, L. H. Wong, J. Barber and J. S. C. Loo, *Energy Environ. Sci.,* 2012, **5**, 5902–5918.
5 A. Züttel, A. Remhof, A. Borgschulte and O. Friedrichs, *Phil. Trans. R. Soc. A*, 2010, **368**, 3329–3342.
6 M. Ball and M. Wietschel, *Intern. J. Hydrogen Energy,* 2009, **34**, 615–627.
7 R. M. Navarro, M. C. Sánchez-Sánchez, M. C. Alvarez-Galvan, F. del Valle and J. L. G. Fierro, *Energy Environ. Sci.,* 2009, **2**, 35–54.

8 K. Christopher and R. Dimitrios, *Energy Environ. Sci.,* 2012, **5**, 6640–6651.
9 C. Acar and I. Dincer, *J. Hydrogen Energy,* 2014, **39**, 1–12.
10 J. D. Holladay, J. Hu, D. L. King and Y. Wang, *Catal. Today*, **139**, 244–260.
11 C. C. Cormos, *Intern. J. Hydrogen Energy,* 2011, **36**, 5960–5971.
12 B. Choi, D. Panthi, M. Nakoji, T. Kabutomori, K. Tsutsumi and A. Tsutsumi, *Intern. J. Hydrogen Energy,* 2015, **40**, 6197–6206.
13 C. Jiao, Z. Huang, X. Wang, H. Zhang, L. Lu and S. Zhang, *RSC Adv.*, 2015, **5**, 34364–34367.
14 P. C. Hallenbeck and J. R. Benemann, *Intern. J. Hydrogen Energy,* 2002, **27**, 1185–1193.
15 M. Wang, Z. Wang, X. Gong and Z. Guo, *Renew. Sustain. Energy Rev.*, 2014, **29**, 573–588.
16 F. Lapicque, J. Lédé and J. Villermaux, *Intern. J. Hydrogen Energy*, 1983, **8**, 675–679.
17 M. A. Rosen, *Energy*, 2010, **35**, 1068–1076.
18 L. Xiao, S. Y. Wu and Y. R. Li, *Renew. Energy*, 2012, **41**, 1–12.
19 S. J. A. Moniz, S. A. Shevlin, D. J. Martin, Z. X. Guo and J. Tang, *Energy Environ. Sci.,* 2015, **8**, 731–759.
20 V. Rosenband and A. Gany, *Intern. J. Hydrogen Energy*, 2010, **35**, 10898–10904.
21 M. Watanabe, *J. Phys. Chem. Solids*, 2010, **71**, 1251–1258.
22 K. Mahmoodi and B. Alinejad, *Intern. J. Hydrogen Energy*, 2010, **35**, 5227–5232.
23 O. V. Kravchenko, L. G. Sevastyanova, S. A. Urvanov and B. M. Bulychev, *Intern. J. Hydrogen Energy*, 2014, **39**, 5522–5527.
24 S. Elitzur, V. Rosenband and A. Gany, *Intern. J. Hydrogen Energy*, 2014, **39**, 6328–6334.
25 S. Mukhopadhyay, G. Rothenberg, H. Wiene and Y. Sasson, *New J. Chem.*, 2000, **24**, 305–308.
26 M. Pudukudy, Z. Yaakob, B. Narayanan, R. Ramakrishnan and S. Viswanathan, *Intern. J. Hydrogen Energy*, 2012, **37**, 7451–7456.
27 D. P. Gregory and J. B. Pangborn, *Annu. Rev. Energy*, 1976, **1**, 279–310.
28 V. Hacker, R. Fankhauser, G. Faleschini, H. Fuchs, K. Friedrich, M. Muhr and K. Kordesch, *J. Power Sources*, 2000, **86**, 531–535.
29 K. Otsuka, T. Kaburagi, C. Yamada and S. Takenaka, *J. Power Sources*, 2003, **122**, 111–121.
30 M. Rydén and M. Arjmand, *Intern. J. Hydrogen Energy*, 2012, **37**, 4843–4854.
31 Y. Wang, F. Jin, X. Zeng, G. Yao and Z. Jing, *Intern. J. Hydrogen Energy*, 2012, **38**, 760–768.
32 K. F. Chen, S. Li and W. X. Zhang, *Chem. Eng. J.*, 2011, **170**, 562–567.

Graphic Abstract

High purity compressed hydrogen gas has been efficiently generated via a facile hydrothermal process of iron powders and water.